PERIDYNAMICS AS AN UPSCALING OF MOLECULAR DYNAMICS[*]

PABLO SELESON[†], MICHAEL L. PARKS[‡], MAX GUNZBURGER[†], AND
RICHARD B. LEHOUCQ[‡]

Abstract. Peridynamics is a formulation of continuum mechanics based on integral equations. It is a nonlocal model, accounting for the effects of long-range forces. Correspondingly, classical molecular dynamics is also a nonlocal model. Peridynamics and molecular dynamics have similar discrete computational structures, as peridynamics computes the force on a particle by summing the forces from surrounding particles, similarly to molecular dynamics. We demonstrate that the peridynamics model can be cast as an upscaling of molecular dynamics. Specifically, we address the extent to which the solutions of molecular dynamics simulations can be recovered by peridynamics. An analytical comparison of equations of motion and dispersion relations for molecular dynamics and peridynamics is presented along with supporting computational results.

Key words. peridynamics, molecular dynamics, upscaling, higher-order gradient

AMS subject classifications. 82D25, 35L75, 70F10, 82C21, 82C22

DOI. 10.1137/09074807X

1. Introduction. Substantial computational challenges are involved in materials science modeling, due to the complexity of the systems of interest. Two principal material descriptions are traditionally utilized. At meso- and macroscales, it is common to use classical continuum mechanics (CCM) models that assume a continuity of matter. For solids, the Cauchy equation of motion,

$$(1.1) \qquad \rho\ddot{\mathbf{u}} = \boldsymbol{\nabla} \cdot \boldsymbol{\sigma} + \mathbf{b},$$

is frequently employed, where $\mathbf{u}$ is a displacement field, $\boldsymbol{\sigma}$ a stress tensor, ρ the mass density, and $\mathbf{b}$ an external body force density. At micro- and nanoscales, molecular dynamics (MD) models may be used; MD provides a discrete description of matter. For an MD system for which atoms interact only via pairwise forces, the equation of motion for atom i is written as

$$(1.2) \qquad m_i\ddot{\mathbf{y}}_i = \sum_{j \neq i} \mathbf{f}_{ij}(\mathbf{y}_i, \mathbf{y}_j) + \mathbf{f}_i^e,$$

where m_i is the mass of atom i, $\mathbf{y}_i$ its position, $\mathbf{f}_{ij}$ the force that atom i feels due to its interaction with atom j, and $\mathbf{f}_i^e$ the external force exerted on atom i. For all

but the smallest systems, MD models are computationally too expensive, whereas CCM models may not accurately resolve microscale phenomena. The need to balance model fidelity with computational cost is a driving motivation for multiscale materials simulations.

One modeling strategy is to *upscale* or *continualize* the MD model, thus replacing inhomogeneities present on smaller length scales by an enhanced continuum description on larger length scales. Our purpose is to develop peridynamics (PD), a nonlocal multiscale continuum theory, as an upscaling of MD so that it preserves characteristic properties of MD models lost by CCM models. The resulting PD models can be solved more cheaply than the corresponding MD models because the PD models can be discretized on a mesh that is coarse with respect to the atomistic lattice.

In section 2, we review the PD model and, in section 3, we present an approach for connecting PD and MD models via higher-order gradient (HOG) models. Starting with an MD model, we derive a corresponding PD model and show that the corresponding HOG equations of motion for both the PD and MD models agree. We provide two specific examples of upscaling MD to PD. In section 4, we upscale a nonlocal linear springs model to PD, showing that both models possess the same HOG equations of motion and the same dispersion relationship, under the appropriate limits. We support our analysis with numerical experiments. We demonstrate in section 4.4.2 that nonlocal models (such as MD or PD) are more dispersive than local models (such as CCM). We also demonstrate in section 4.4.3 that this additional dispersion acts to regularize the solution. In section 5 we present the upscaling of a Lennard-Jones model to PD, again with supporting numerical experiments. Conclusions are presented in section 6.

2. The peridynamics model. Peridynamics was proposed in [27] as a nonlocal reformulation of solid mechanics. By nonlocal, we mean that continuum points separated by a finite distance may exert force upon each other. The PD model is based on an integral representation of the internal force density acting on a material point and does not assume even weak differentiability of the displacement field, in contrast to CCM models (cf. (1.1)). Dependence upon the differentiability of the displacement field limits the direct applicability of CCM models, whereas discontinuous displacements represent no mathematical or computational difficulty for PD. Consequently, PD has frequently been applied in the study of material failure [5]. PD is a member of a larger class of nonlocal formulations of solid mechanics. See, e.g., Kröner [15], Kunin [17, 18], and Rogula [23], and the references cited therein.

2.1. Kinematics. Let a body in some reference configuration occupy a region $\mathcal{B}$, as in Figure 2.1. For any $\mathbf{x} \in \mathcal{B}$, the PD equation of motion is [27]

$$(2.1) \qquad \rho(\mathbf{x})\ddot{\mathbf{u}}(\mathbf{x},t) = \int_{\mathcal{H}_{\mathbf{x}}} \boldsymbol{\kappa}\left(\mathbf{u}(\mathbf{x}',t) - \mathbf{u}(\mathbf{x},t), \mathbf{x}' - \mathbf{x}\right) dV_{\mathbf{x}'} + \mathbf{b}(\mathbf{x},t), \quad t \geq 0,$$

where $\mathcal{H}_{\mathbf{x}}$ is known as the *neighborhood* of $\mathbf{x}$ (i.e., a spherical region of radius δ around $\mathbf{x}$, where δ is called the *horizon*), $\rho(\mathbf{x})$ the mass density, and $\mathbf{b}(\mathbf{x},t)$ the body force density. Let $\mathbf{u} \equiv \mathbf{u}(\mathbf{x},t)$ denote the displacement field with initial conditions $\mathbf{u}(\mathbf{x},0) = \mathbf{u}_0(\mathbf{x})$, $\dot{\mathbf{u}}(\mathbf{x},0) = \dot{\mathbf{u}}_0(\mathbf{x})$. Let $\mathbf{y} \equiv \mathbf{y}(\mathbf{x},t) = \mathbf{x} + \mathbf{u}(\mathbf{x},t)$ denote the position at time t of a particle that was at $\mathbf{x}$ in the reference configuration. The vector function $\boldsymbol{\kappa}(\mathbf{u}' - \mathbf{u}, \mathbf{x}' - \mathbf{x})$ denotes the force density per unit reference volume exerted on a point $\mathbf{y}$ by the point $\mathbf{y}'$ along the line between them.

We emphasize that the PD model is a *nonlocal* model that allows *action-at-a-distance*. The point $\mathbf{x}$ interacts with all points $\mathbf{x}' \in \mathcal{H}_{\mathbf{x}}$ through $\boldsymbol{\kappa}$. Due to the
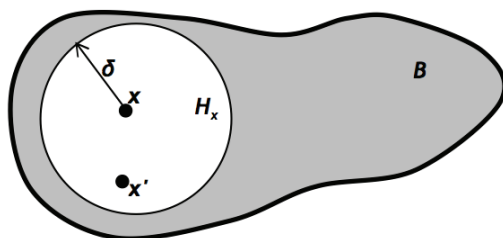
FIG. 2.1. *Peridynamics body* $\mathcal{B}$*.* $\mathcal{H}_{\mathbf{x}}$ *is known as the* neighborhood *of* $\mathbf{x}$*, i.e., a spherical region of radius* δ *around* $\mathbf{x}$*, where* δ *is called the* horizon*. The points* $\mathbf{x}$*,* $\mathbf{x}'$ *interact via the pairwise function* $\boldsymbol{\kappa}$*; see* (2.1)*.*

similarity of the force evaluation with MD, the PD model has sometimes been called a "continuum" formulation of MD [27].

The constitutive relationship for any specific *macroscopic* material is contained within $\boldsymbol{\kappa}$. For more information about constitutive modeling with PD, we refer the reader to [27, 28, 29]. In this paper, we focus only on determining $\boldsymbol{\kappa}$ from an upscaling of MD. However, we note the basic requirements that $\boldsymbol{\kappa}$ must possess to conserve linear and angular momentum, namely that

$$\boldsymbol{\kappa}(\mathbf{u} - \mathbf{u}', \mathbf{x} - \mathbf{x}') = -\boldsymbol{\kappa}(\mathbf{u}' - \mathbf{u}, \mathbf{x}' - \mathbf{x}) \quad \text{and} \quad (\mathbf{y}' - \mathbf{y}) \times \boldsymbol{\kappa}(\mathbf{u}' - \mathbf{u}, \mathbf{x}' - \mathbf{x}) = 0$$

for all $\mathbf{x}, \mathbf{x}', \mathbf{u}, \mathbf{u}'$ [22, 27].

The kernels $\boldsymbol{\kappa}$ introduced in this paper (and discussed above) assume pairwise forces. A more general class of interactions $\boldsymbol{\kappa}$ was introduced in [29].

2.2. Discretization. There are many possible ways to discretize (2.1); see [13] for an overview. Here, we use the meshfree discretization discussed in [28].

The body $\mathcal{B}$ is discretized into cubic subregions; although this implies a "staircase" approximation to the boundary of $\mathcal{B}$, this is sufficient for the purposes of this paper. Denote the position of the center of subregion i in the reference configuration by $\mathbf{x}_i$ and by $\mathbf{y}_i$ in the deformed configuration at time t. We refer to the subregions' centers as "particles." Further, for the subregion corresponding to the point i, let

$$(2.2) \qquad\qquad \mathcal{F}_i = \{ j \mid \|\mathbf{x}_j - \mathbf{x}_i\| \leq \delta, j \neq i \}$$

denote the family of particles within a distance δ of particle i in the reference configuration. We may then write the semidiscrete equation of motion for the subregion containing point i as

$$(2.3) \qquad\qquad \rho_i \ddot{\mathbf{u}}_i = \sum_{j \in \mathcal{F}_i} \boldsymbol{\kappa}(\mathbf{u}_j - \mathbf{u}_i, \mathbf{x}_j - \mathbf{x}_i) V_j + \mathbf{b}_i,$$

where V_j is the volume of subregion j, $\rho_i \equiv \rho(\mathbf{x}_i)$, $\mathbf{u}_i \equiv \mathbf{u}(\mathbf{x}_i, t)$, and $\mathbf{b}_i \equiv \mathbf{b}(\mathbf{x}_i, t)$. We may view the summation in (2.3) as a quadrature of the integral in (2.1).

The semidiscrete equation (2.3) may be discretized in time by any suitable scheme. We choose the velocity Verlet method. This particular discretization of the semidiscrete PD model (2.3) has the same computational structure as MD so that it lends itself well to implementation within an MD framework. For implementation details of PD within the LAMMPS MD code, see [22].

3. Upscaling molecular dynamics to peridynamics. Because the PD model (2.1) is similar to MD and its semidiscretization (2.3) has the same computational structure as MD, it is natural to attempt to cast PD as an upscaling of MD.

Our goal is to deduce a continuum PD model that can recover the same dynamics as a given MD model. For that purpose, we need to find kernels κ corresponding to specific MD interactions. There are many different mechanisms for deriving κ from an MD model. For a given MD model, is one κ better than another? Our work is motivated by a desire to address this question. To this end, we observe that HOG models (discussed below) can be derived from both MD and PD models. Under the assumption that MD and PD models that produce the same HOG model possess the same dynamics, we can use HOG models as a bridge to connect PD to MD, thus effecting an upscaling from MD to PD. The general approach is diagrammed in Figure 3.1, where the HOG model is presented as a tool to establish a correspondence between MD and PD.
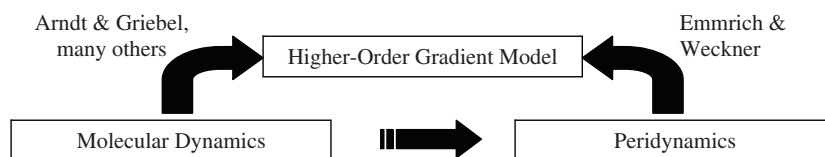

Fig. 3.1. *Connection between a molecular dynamics (MD) and a peridynamics (PD) model through a higher-order gradient (HOG) model. Passage from an MD model to a HOG model is described in* [4] *and elsewhere. Passage from a PD model to a HOG model is described in* [12]. *A PD model is an upscaling of an MD model if both produce the same HOG model.*

We emphasize that we are not interested in doing numerical simulations with HOG models, but use them only as an analytical tool to connect MD and PD models. Once correspondence between given MD and PD models is established, we discard the associated HOG model and perform computations with the PD model. We prefer a PD model to a HOG model for the reason discussed in section 2, i.e., that the PD model requires fewer assumptions on the smoothness of the displacement field.

We summarize our process for upscaling MD to PD:
1. Choose an MD model, i.e., choose $\mathbf{f}_{ij}$ in (1.2).
2. Select a PD model, i.e., choose κ in (2.1).
3. Derive HOG models for both the MD and PD models.
4. Compare the two HOG models. Equality indicates that the PD model is an upscaling of the MD model.

In section 3.1, we introduce HOG models using a simple example and discuss the role of length scales in both nonlocal models and HOG models. In section 3.2, we describe in more detail the passage from an MD model to a HOG model.

3.1. Higher-order gradient models, length scales, and nonlocality. The Cauchy equation of motion for a solid (1.1) does not possess a length scale if the stress tensor σ depends only on the gradient of $\mathbf{u}$. Consequently, such a model cannot represent dynamics on macro- and mesoscales while simultaneously representing smaller length-scale behavior. Such classical models can be enhanced to describe the underlying microstructure or nanostructure by augmenting the governing constitutive relations to produce what is referred to as *higher-order continua*. Introduction of higher-order spatial derivatives introduces multiple additional length scales; it is these length scales that allow for representation of the micro- and nanoscales [6].

Considerable work has been accomplished in the development of higher-order continuum models that have been used to model many experimentally observed phenomena such as localized deformation (shear banding) [7], strain softening [10], etc. See [1] for an overview. In particular, much effort has been put forth in deriving higher-order continua from discrete or granular media; see, e.g., [2, 4, 6, 7, 10, 16, 20, 21, 24, 25, 26, 31, 32, 33, 34, 36]. Many, if not all, of these works consider preserving in the higher-order continuum model the dispersive effects present in the discrete model. These dispersive effects arise because discrete models are, by definition, spatially inhomogeneous. Any small-scale spatial inhomogeneity in a meso- or macroscale object will manifest itself in multiscale behavior. The underlying fine-scale model need not be discrete to produce solutions with multiple length or time scales. Such an example is considered in [11], where a continuum macroscale material with a periodic microstructure is considered.

To motivate later sections, we present here simple one-dimensional equations and identify the associated length scales. Consider the classical wave equation

$$\frac{\partial^2 y}{\partial t^2} = a \frac{\partial^2 y}{\partial x^2}, \tag{3.1}$$

which does not possess a length scale. Its solutions are *scale-invariant* in the sense of Barenblatt [8]. Now consider the higher-order wave equation

$$\frac{\partial^2 y}{\partial t^2} = a \frac{\partial^2 y}{\partial x^2} - b \frac{\partial^4 y}{\partial x^4}, \tag{3.2}$$

where a and b are constant coefficients.[1] Dimensional consistency of the terms in (3.2) ensures that the equation has a length scale, and that scale is $L = \sqrt{b/a}$. We can rescale space, i.e., rescale x, to be either large or small relative to L, and thus make either the first or second term in the right-hand side of (3.2) dominant. Solutions of (3.2) are *not* scale-invariant; they change as a function of the length scale to which the PDE is applied. In this sense, we refer to (3.2) as a *multiscale* equation.

We emphasize that equations (3.1) and (3.2) are *local* equations, in contrast to (2.1), which is a nonlocal equation. Here, "local" means that each term in the equation (e.g., $\partial^2 y/\partial x^2$) depends only upon x.

Under the assumption that the displacement field $\mathbf{u}$ is sufficiently smooth, the nonlocal PD model (2.1) is equivalent to a local HOG PDE, as suggested in Figure 3.1. It is shown in [12] that one can write (2.1) as a HOG model by performing a series expansion of $\mathbf{x}' - \mathbf{x}$ about $\mathbf{x}$ within κ, and then integrating over $\mathcal{H}_{\mathbf{x}}$ directly. We refer the reader to [12] for the details.

In comparing (3.1) to (3.2), we note that the d'Alembert solution to (3.1) does not result in dispersion of the initial condition (cf. Figures 4.3(b) and 4.4(b)), while dispersion is clearly present in the solution to (3.2), as we will see in section 4. This dispersion present in HOG models acts to regularize the solution. When one can equate nonlocal integral models to HOG models, nonlocal integral models such as (2.1) must also possess this regularizing effect.

We have stated that a model must possess a length scale in order to exhibit multiscale behavior and have indicated how to identify that length scale within a HOG PDE such as (3.2). We observe here that (2.1) also has a length scale δ, the PD horizon. By altering this length scale, we change the solution in the same manner

---

[1]To avoid the well-known "bad-sign" problem, we assume that $a > 0$ and $b > 0$. See [24].

as discussed for (3.2). For a simple example of the effect of altering δ, note that in the limit $\delta \to 0$, it is shown in [12, 30] that, under certain assumptions, the PD model (2.1) converges to the equation of classical elasticity. Below, we demonstrate analogous results and show how an appropriate choice of the length scale in a PD model can preserve the dynamics of an MD model.

3.2. Upscaling molecular dynamics to a higher-order gradient model. Although many methods have been presented for passing from a discrete media to a continuum equation, we will concern ourselves only with the "inner expansion" technique introduced in [4]. This method avoids complications of other continualization approaches. Most notably, it avoids producing ill-posed HOG models such as the "bad-sign" equation mentioned earlier. We briefly review the inner expansion technique here and refer the reader to [3, 4] for a complete discussion.

Consider a system of N atoms with interactions described by the potential energy function

$$\Phi^{(A)} = \Phi^{(A)}(\{\mathbf{y}_i\}_{i=1,\dots,N_x}),$$

with N_x the number of atoms in the system, $\mathbf{y}_i \in \mathbb{R}^d$ the atom positions, and d the spatial dimension. In the reference configuration, the atoms occupy a set of points $\{\mathbf{x}\}$ on a lattice $\mathcal{L}$. Assuming the domain $\Omega \subset \mathbb{R}^d$ describes the undeformed form of a crystal, we can express the potential energy of the deformed crystal as

$$\Phi^{(A)} = \Phi^{(A)}(\{\mathbf{y}(\mathbf{x})\}_{\mathbf{x}\in\mathcal{L}\cap\Omega}).$$

Under the assumption that the potential energy can be split into a sum of local interactions $\Phi^{(A),\overline{\mathbf{x}}}$ around some point $\overline{\mathbf{x}}$, we can write

$$\Phi^{(A)}(\{\mathbf{y}(\mathbf{x})\}_{\mathbf{x}\in\mathcal{L}\cap\Omega}) = \sum_{\overline{\mathbf{x}}\in\overline{\mathcal{L}}\cap\Omega} \Phi^{(A),\overline{\mathbf{x}}}(\{\mathbf{y}(\mathbf{x})\}_{\mathbf{x}\in\mathcal{L}\cap\Omega}),$$

with $\{\overline{\mathbf{x}}\}$ a set of points on an associated lattice $\overline{\mathcal{L}}$.

We consider a Taylor expansion of the deformation function $\mathbf{y}$ around $\overline{\mathbf{x}}$ up to some degree $K \in \mathbb{N}$ as

$$(3.3) \qquad \mathbf{y}(\mathbf{x}) \approx \sum_{k=0}^{K} \frac{1}{k!} \nabla^k \mathbf{y}(\overline{\mathbf{x}}) : (\mathbf{x} - \overline{\mathbf{x}})^k,$$

where the colon denotes the higher-dimensional scalar product. To reduce the remainder term in the Taylor series, a particular choice can be used for $\overline{\mathbf{x}}$. There is an optimal choice for $\overline{\mathbf{x}}$, in the case where the local potential $\Phi^{(A),\overline{\mathbf{x}}}$ depends on a linear combination of all components of all points $\mathbf{y}(\mathbf{x})$ such that

$$\Phi^{(A),\overline{\mathbf{x}}}(\{\mathbf{y}(\mathbf{x})\}_{\mathbf{x}\in\mathcal{L}\cap\Omega}) = \varphi\left(\sum_{\mathbf{x}\in\mathcal{L}\cap\Omega} a_{\mathbf{x}} \cdot \mathbf{y}(\mathbf{x})\right),$$

with $\varphi : \mathbb{R} \to \mathbb{R}$ a function and $a_{\mathbf{x}} \in \mathbb{R}^d$ constants for all $\mathbf{x} \in \mathcal{L} \cap \Omega$. This choice is found to be the barycenter

$$\overline{\mathbf{x}} = \frac{\sum_{\mathbf{x}\in\mathcal{L}\cap\Omega} |a_{\mathbf{x}}|\mathbf{x}}{\sum_{\mathbf{x}\in\mathcal{L}\cap\Omega} |a_{\mathbf{x}}|}.$$

Using the Taylor expansion (3.3) we can express the local potential $\Phi^{(A),\overline{\mathbf{x}}}$ as

$$\Phi^{(A),\overline{\mathbf{x}}}(\{\mathbf{y}(\mathbf{x})\}_{\mathbf{x}\in\mathcal{L}\cap\Omega}) \approx \Phi^{(A),\overline{\mathbf{x}}}\left(\left\{\sum_{k=0}^{K}\frac{1}{k!}\nabla^k\mathbf{y}(\overline{\mathbf{x}}):(\mathbf{x}-\overline{\mathbf{x}})^k\right\}_{\mathbf{x}\in\mathcal{L}\cap\Omega}\right),$$
$$= \Phi^{(I),\overline{\mathbf{x}}}\left(\mathbf{y}(\overline{\mathbf{x}}),\nabla\mathbf{y}(\overline{\mathbf{x}}),\nabla^2\mathbf{y}(\overline{\mathbf{x}}),\ldots,\nabla^K\mathbf{y}(\overline{\mathbf{x}})\right),$$

where $\Phi^{(I),\overline{\mathbf{x}}}$ is defined as

$$\Phi^{(I),\overline{\mathbf{x}}}(\mathbf{d}^0,\mathbf{d}^1,\mathbf{d}^2,\ldots,\mathbf{d}^K) \equiv \Phi^{(A),\overline{\mathbf{x}}}\left(\left\{\sum_{k=0}^{K}\frac{1}{k!}\mathbf{d}^k:(\mathbf{x}-\overline{\mathbf{x}})^k\right\}_{\mathbf{x}\in\mathcal{L}\cap\Omega}\right).$$

Note that the original potential $\Phi^{(A),\overline{\mathbf{x}}}$ depends on the deformation $\mathbf{y}$ at all the lattice points $\mathbf{x}\in\mathcal{L}\cap\Omega$, while the new representation $\Phi^{(I),\overline{\mathbf{x}}}$ depends only on the value of $\mathbf{y}$ and its derivatives at $\overline{\mathbf{x}}$. We have replaced a nonlocal model with its local approximation.

The total potential is obtained (up to the approximated degree K) by

$$\Phi^{(I)}(\mathbf{y}) = \sum_{\overline{\mathbf{x}}\in\overline{\mathcal{L}}\cap\Omega}\Phi^{(I),\overline{\mathbf{x}}}\left(\mathbf{y}(\overline{\mathbf{x}}),\nabla\mathbf{y}(\overline{\mathbf{x}}),\nabla^2\mathbf{y}(\overline{\mathbf{x}}),\ldots,\nabla^K\mathbf{y}(\overline{\mathbf{x}})\right).$$

A continuous expression for the continuum potential energy is then obtained by replacing the discrete (Riemann) sum with its continuous integral representation, as

$$(3.4) \qquad \Phi^{(C)}(\mathbf{y}) = \frac{1}{V}\int_\Omega \Phi^{(I),\overline{\mathbf{x}}}\left(\mathbf{y}(\overline{\mathbf{x}}),\nabla\mathbf{y}(\overline{\mathbf{x}}),\nabla^2\mathbf{y}(\overline{\mathbf{x}}),\ldots,\nabla^K\mathbf{y}(\overline{\mathbf{x}})\right)d\overline{\mathbf{x}},$$

where V is the volume of a unit cell of the lattice. Finally, we can write

$$\Phi^{(C)}(\mathbf{y}) = \int_\Omega \Phi^{(C),\mathbf{x}}\left(\mathbf{y}(\mathbf{x}),\nabla\mathbf{y}(\mathbf{x}),\nabla^2\mathbf{y}(\mathbf{x}),\ldots,\nabla^K\mathbf{y}(\mathbf{x})\right)d\mathbf{x},$$

where $\Phi^{(C),\mathbf{x}} \equiv \frac{1}{V}\Phi^{(I),\mathbf{x}}$, which represents the potential energy density, and we replaced $\overline{\mathbf{x}}$ by $\mathbf{x}$ since $\overline{\mathbf{x}}$ is a dummy variable in (3.4).

The resulting equation of motion is [4]

$$\rho\frac{\partial^2\mathbf{y}}{\partial t^2} = \sum_{k=0}^{K}(-1)^{k+1}\mathrm{div}^k\Phi_{,k}^{(C),\mathbf{x}}\left(\mathbf{y}(\mathbf{x}),\nabla\mathbf{y}(\mathbf{x}),\nabla^2\mathbf{y}(\mathbf{x}),\ldots,\nabla^K\mathbf{y}(\mathbf{x})\right) \qquad \text{in } \Omega,$$

where $\Phi_{,k}^{(C),\mathbf{x}}$ denotes the derivative of $\Phi^{(C),\mathbf{x}}$ with respect to the argument $\nabla^k\mathbf{y}(\mathbf{x})$. The above equation requires appropriate initial values and boundary conditions.

4. Nonlocal linear springs model. In this section, we aim to find a PD model corresponding to a toy one-dimensional nonlocal linear springs MD model. We compare both models through HOG continuum equations of motion, and show that the dispersion relations obtained from both models match. For comparison, we show that the HOG continuum model derived from a local (nearest neighbor) linear springs MD model does not match the HOG model derived from a nonlocal linear springs MD model.

Our one-dimensional MD model consists of a nonlocal chain of atoms. Each atom is assumed to have a mass m, and is connected to N neighbors on each side with linear
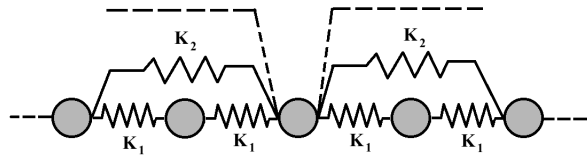
FIG. 4.1. *Nonlocal linear springs molecular dynamics system. Each atom is connected with N neighbors on each side through linear springs, with spring constants K_j, $j = 1, \ldots, N$.*

springs, as illustrated in Figure 4.1. Let a be the lattice constant, and let the spring constant between an atom and its jth neighbor be $K_j = K(N)/|ja|$, where $K(N)$ is a function of the number of neighbor interactions N. The spring constant decreases as the equilibrium bond length increases. Here and in the remainder of this paper we assume that there is no external force, i.e., $\mathbf{f}_i^e \equiv \mathbf{0}$ in (1.2), and correspondingly $\mathbf{b}(\mathbf{x}, t) \equiv \mathbf{0}$ in (2.1). The equation of motion is

$$(4.1) \qquad m\ddot{y}(x_i, t) = \sum_{\substack{j=-N \\ j \neq 0}}^{N} \frac{K(N)}{|ja|} \Big[y(x_i + ja, t) - y(x_i, t) - ja \Big], \quad i = 1, \ldots, N_x,$$

where N_x is the number of atoms in the system, and $y(x_i, t)$ is the current position at time t of an atom which was at x_i in the reference configuration.

4.1. Higher-order gradient continuum models. To develop a HOG PDE for (4.1), we first write the local potential $\Phi^{(A), \overline{x}}$ (see section 3.2) as

$$\Phi^{(A), \overline{x}} = \begin{cases} \displaystyle\sum_{j=1}^{\lfloor \frac{N}{2} \rfloor} \frac{1}{2} \frac{K(N)}{|2ja|} \left(y\left(\overline{x} + ja, t\right) - y\left(\overline{x} - ja, t\right) - 2ja \right)^2 & \text{if } \frac{\overline{x}}{a} \in \mathbb{Z} \cap \Omega, \\[2em] \displaystyle\sum_{j=1}^{\lceil \frac{N}{2} \rceil} \frac{1}{2} \frac{K(N)}{|(2j-1)a|} \left(y\left(\overline{x} + ja - \frac{a}{2}, t\right) \right. \\ \qquad\qquad \left. - y\left(\overline{x} - ja + \frac{a}{2}, t\right) - (2j-1)a \right)^2 & \text{if } \frac{\overline{x}}{a} \in \left(\mathbb{Z} + \frac{1}{2}\right) \cap \Omega. \end{cases}$$

We apply the inner expansion presented in section 3.2 to produce the equation of motion

$$\rho \frac{\partial^2 y}{\partial t^2} = \frac{2K(N)}{a^2} \left[\left(\sum_{j=1}^{N} j \right) \frac{a^2}{2!} \frac{\partial^2 y}{\partial x^2} + \left(\sum_{j=1}^{N} j^3 \right) \frac{a^4}{4!} \frac{\partial^4 y}{\partial x^4} + \left(\sum_{j=1}^{N} j^5 \right) \frac{a^6}{6!} \frac{\partial^6 y}{\partial x^6} + \cdots \right],$$

where we used the mass-density relation $m = \rho a$, and we have introduced partial derivatives since now y is being viewed as a continuum function of x and t. Furthermore, the dependence on x and t is omitted for simplicity. We first apply closed-form expressions for the summations and take $N \gg 1$, keeping only the dominant terms, to obtain the HOG PDE

$$(4.2) \qquad \frac{\partial^2 y}{\partial t^2} = \frac{K_1}{\rho} \left[\frac{\partial^2 y}{\partial x^2} + \frac{(Na)^2}{24} \frac{\partial^4 y}{\partial x^4} + \frac{(Na)^4}{1080} \frac{\partial^6 y}{\partial x^6} + \cdots \right],$$

with $K(N) = 2K_1/(N(N+1))$ (see Appendix A.1). The expression (4.2) agrees with the HOG PDE (4.4) derived below for the PD model.

We will conjecture that the PD equation of motion for our one-dimensional up-scaled model is (see Appendix A.1)

$$(4.3) \qquad \rho(x)\frac{\partial^2 y}{\partial t^2}(x,t) = \int_{-\delta}^{\delta} \frac{c}{|\varepsilon|}(y(x+\varepsilon,t) - y(x,t) - \varepsilon)\mathrm{d}\varepsilon.$$

Following [12], we use a Taylor expansion to get the expression

$$\rho\frac{\partial^2 y}{\partial t^2} = \int_{-\delta}^{\delta} \frac{c}{|\varepsilon|}\left(\frac{\partial y}{\partial x}\varepsilon + \frac{1}{2!}\frac{\partial^2 y}{\partial x^2}\varepsilon^2 + \frac{1}{3!}\frac{\partial^3 y}{\partial x^3}\varepsilon^3 + \frac{1}{4!}\frac{\partial^4 y}{\partial x^4}\varepsilon^4 + \cdots - \varepsilon\right)\mathrm{d}\varepsilon.$$

Performing the integration and exploiting symmetry gives

$$(4.4) \qquad \frac{\partial^2 y}{\partial t^2} = \frac{K_1}{\rho}\left[\frac{\partial^2 y}{\partial x^2} + \frac{\delta^2}{24}\frac{\partial^4 y}{\partial x^4} + \frac{\delta^4}{1080}\frac{\partial^6 y}{\partial x^6} + \cdots\right],$$

where the relation $c = 2K_1/\delta^2$ (see Appendix A.1) was used. We have recovered (4.2), the same HOG PDE as in the nonlocal MD case by preserving the nonlocality of the model, i.e., setting $\delta = Na$. We have matched the equations of motion (4.2) and (4.4) to the sixth order, although this can be done to arbitrary order.

For comparison, we now derive the HOG continuum model for a *local* linear springs model. The equation of motion for a nearest neighbor interaction is

$$(4.5) \qquad m\ddot{y}(x_i,t) = \sum_{\substack{j=-1 \\ j\neq 0}}^{1} \frac{K_1}{a}\Big[y(x_i+ja,t) - y(x_i,t) - ja\Big], \qquad i = 1,\ldots,N_x.$$

Following the same procedure as above, we obtain the HOG PDE

$$(4.6) \qquad \frac{\partial^2 y}{\partial t^2} = \frac{K_1}{\rho}\left[\frac{\partial^2 y}{\partial x^2} + \frac{a^2}{12}\frac{\partial^4 y}{\partial x^4} + \frac{a^4}{360}\frac{\partial^6 y}{\partial x^6} + \cdots\right].$$

The general form of (4.6) is similar to (4.4), though the coefficients differ. In particular, (4.4) has coefficients that depend on the horizon δ, while in (4.6) the coefficients depend on the lattice constant a. Thus, in the continuum limit ($a \to 0$), (4.6) reduces to the classical wave equation

$$(4.7) \qquad \frac{\partial^2 y}{\partial t^2} = \frac{K_1}{\rho}\frac{\partial^2 y}{\partial x^2},$$

in contrast to the nonlocal model (4.1) which preserves the HOG terms in (4.2) in the continuum limit, when Na is held constant. In the local limit ($\delta \to 0$), our nonlocal PD model (4.3) converges to the classical wave equation (4.7), showing that in this case PD converges to classical elasticity [12, 30].[2]

4.2. Dispersion relations. To obtain the dispersion relation for the nonlocal model (4.1), we set $y(x,t) = x + e^{i(kx+\omega t)}$ to get

$$\omega^2 = \sum_{j=1}^{N} 2\frac{K(N)}{m}\frac{1}{ja}\Big[1 - \cos(kja)\Big].$$

---

[2]We interpret the limits $a \to 0$ and $\delta \to 0$ to mean a rescaling of our equations in relation to some externally defined length scale L. We keep the atomistic length scale a constant and change the scale L of our system such that $a/L \to 0$ and $\delta/L \to 0$, respectively.

We assume $kNa \ll 1$, i.e., the wavelength of the signal $\lambda = 2\pi/k$ is much longer than the maximum interaction distance Na. Under this assumption, we can apply a Taylor expansion for every j and get

$$\omega^2 = 2\frac{K(N)}{m}\left[\left(\sum_{j=1}^{N} j\right)\frac{ak^2}{2!} - \left(\sum_{j=1}^{N} j^3\right)\frac{a^3k^4}{4!} + \left(\sum_{j=1}^{N} j^5\right)\frac{a^5k^6}{6!} - \left(\sum_{j=1}^{N} j^7\right)\frac{a^7k^8}{8!} + \cdots\right].$$

We use again the mass-density relation $m = \rho a$, and a Taylor expansion for the function $\sqrt{1+x}$. Furthermore, we substitute closed-form expressions for the summations and take $N \gg 1$, i.e., the number of neighbor interactions is very large. Keeping only the dominant terms gives

$$(4.8) \qquad \omega = \sqrt{\frac{K_1}{\rho}}k\left[1 - \frac{1}{48}(kNa)^2 + \frac{17}{69120}(kNa)^4 + \cdots\right],$$

where the relation $K(N) = 2K_1/(N(N+1))$ (see Appendix A.1) was used. This result agrees with the dispersion relation (4.9) obtained for the upscaled PD model (4.3). Note that the assumptions $N \gg 1$ and $kNa \ll 1$ are both satisfied in the continuum limit for long wavelengths, when Na remains constant. For a nearest neighbor interaction ($N = 1$), in the continuum limit, we get $\omega \approx (\sqrt{K_1/\rho})k$, the dispersion relation for the classical wave equation (4.7), with $\sqrt{K_1/\rho}$ as the wave speed.

We now derive the corresponding dispersion relation for the PD model. Substitute $y(x,t) = x + e^{i(kx+\omega t)}$ into (4.3) to get the dispersion relation [35]

$$\omega^2 = \int_0^\delta 2\frac{c}{\rho\varepsilon}(1 - \cos(k\varepsilon))d\varepsilon.$$

We assume $k\delta \ll 1$, i.e., the wavelength of the signal $\lambda = 2\pi/k$ is much longer than the horizon δ. After a Taylor expansion and integration we obtain the relation

$$\omega^2 = 2\frac{c}{\rho}\left(\frac{k^2\delta^2}{2!2} - \frac{k^4\delta^4}{4!4} + \frac{k^6\delta^6}{6!6} + \cdots\right).$$

Using a Taylor expansion for the function $\sqrt{1+x}$, we get

$$(4.9) \qquad \omega = \sqrt{\frac{K_1}{\rho}}k\left[1 - \frac{1}{48}(k\delta)^2 + \frac{17}{69120}(k\delta)^4 + \cdots\right],$$

with $c = 2K_1/\delta^2$ (see Appendix A.1). This result is consistent with the dispersion relation (4.8) for the nonlocal MD model when $Na = \delta$, preserving the nonlocality of the model. Our upscaled PD model (4.3) has the same dispersion relationship as that of the MD model (4.1).

4.3. Stability analysis. We perform a stability analysis on the velocity Verlet algorithm implemented on our MD and the discretized PD and CCM models. Our stability analysis follows that for PD in [28]. We use this analysis to choose a refinement path for our numerical experiments in section 4.4.

Following [14], instead of performing the stability analysis on the velocity Verlet algorithm, we perform it on the equivalent equation

$$(4.10) \qquad m\frac{y_j^{n+1} - 2y_j^n + y_j^{n-1}}{(\Delta t)^2} = \sum_p F_{p,j},$$

with m the particle mass, Δt the time step, $y_j^n \equiv y(x_j, t^n)$ the position at time t^n of a particle that was at x_j in the reference configuration, and $F_{p,j}$ the force that particle p exerts on particle j. Following our MD model (4.1), we implement a linear spring force of the form

$$F_{p,j} = \frac{K(N)}{|x_p - x_j|} \left((y_p - y_j) - (x_p - x_j) \right),$$

where the force constant K depends on the number of neighbor interactions N. As we are interested in mesh refinement and thus prefer to work with densities instead of masses, we replace m by $\rho \Delta x$ in (4.10), with ρ the mass density of the system and Δx the spatial resolution. We let $y_j^n = x_j + \zeta^n e^{ikj\Delta x}$, obtaining

$$\frac{\rho}{(\Delta t)^2} \left(\zeta - 2 + \zeta^{-1} \right) = \sum_{\substack{p=j-N \\ p \neq j}}^{j+N} \frac{K(N)}{|p - j| (\Delta x)^2} \left(e^{ik(p-j)\Delta x} - 1 \right).$$

Using the notation $q = p - j$, we write

$$\frac{\rho}{(\Delta t)^2} \left(\zeta - 2 + \zeta^{-1} \right) = \sum_{\substack{q=-N \\ q \neq 0}}^{N} \frac{K(N)}{|q| (\Delta x)^2} \left(e^{ikq\Delta x} - 1 \right)$$

$$= \sum_{q=1}^{N} 2 \frac{K(N)}{q(\Delta x)^2} \left(\cos(kq\Delta x) - 1 \right) \equiv -2M_k,$$

and notice that $M_k \geq 0$. This reduces to the quadratic equation

(4.11) $$\zeta^2 - 2 \left(1 - M_k \frac{(\Delta t)^2}{\rho} \right) \zeta + 1 = 0.$$

Solving (4.11) and requiring that $|\zeta| \leq 1$ leads to the inequality

$$\Delta t < \sqrt{2\rho/M_k} = \sqrt{\frac{2\rho}{\sum_{q=1}^{N} \frac{K(N)}{q(\Delta x)^2} \left(1 - \cos(kq\Delta x) \right)}}.$$

By replacing $(1 - \cos(kq\Delta x))$ by 2, we ensure that the above condition is satisfied for all k. This leads to the stability condition

(4.12) $$\Delta t < \sqrt{\frac{\rho}{K(N) \sum_{q=1}^{N} \frac{1}{q}}} \Delta x.$$

This will provide an appropriate refinement path for our numerical experiments in section 4.4.

We now focus on (4.12), and apply the relation $K(N) = \frac{2K_1}{N(N+1)}$ (see Appendix A.1). In addition, we use the relation $N\Delta x = \delta$ to get

$$\Delta t < \delta \sqrt{\frac{\rho}{2K_1}} \sqrt{\frac{1 + \frac{1}{N}}{\sum_{q=1}^{N} \frac{1}{q}}}.$$

For $N \gg 1$, we can approximate the harmonic number $H_N \equiv \sum_{q=1}^{N} \frac{1}{q} \approx \ln(N) + \gamma$, where $\gamma > 0$ is the Euler–Mascheroni constant. Then, we can express the above condition as

$$\Delta t < \delta \sqrt{\frac{\rho}{2K_1}} \sqrt{\frac{1 + \frac{1}{N}}{\ln(N) + \gamma}} \approx \delta \sqrt{\frac{\rho}{2K_1}} \sqrt{\frac{1}{\ln(N)}} \approx \delta \sqrt{\frac{\rho}{2K_1}} \frac{1}{\sqrt{\ln\left(\frac{1}{\Delta x}\right)}},$$

where we assumed $\ln(1/\Delta x) \gg \ln(\delta)$ in the rightmost approximation. It is straightforward to show that $1/\sqrt{\ln(1/\Delta x)} > \Delta x$; therefore, our stability condition implies that the dependence of Δt on Δx is weaker than the classical Courant–Friedrichs–Lewy (CFL) condition for the wave equation that requires $\Delta t = O(\Delta x)$ as $\Delta x \to 0$. On the other hand, in the limit $1/\Delta x \gg \delta$, our stability condition reduces to $\Delta t = O(\delta)$. These results are consistent with the results presented in [28].

The dependence of the time step on the spatial resolution is illustrated in Figure 4.2 for the choices $\delta = 5$, $\rho = 1.0$, and $K_1 = 1.0$, using relation (4.13) with $\Delta t_0 = 1$ (solid line with dots). In comparison, we show a linear dependence between Δt and Δx (dashed line), and we see that the condition (4.12) is weaker than the CFL condition; i.e., larger time steps are allowed for a given spatial resolution in the case of small values of Δx. Furthermore, we notice that this bound ensures stability for all wavenumbers k. Thus, we expect the stability limit to be slightly larger in practice. The numerically determined experimental stability limit for the case of the square pulse (4.14) was computed for different values of Δx and the results are presented in the same figure for comparison (dashed line with plus signs). We see that for small values of Δx, we are allowed to increase the time step by about 20–30% beyond the stability limit (4.12).
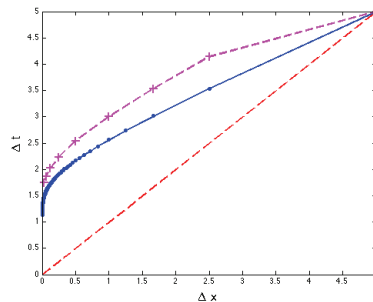

FIG. 4.2. *Dependence of the time step (Δt) on the spatial resolution (Δx). The stability condition (4.12) (solid line with dots) is compared with a linear dependence between Δt and Δx (dashed line). In addition, the numerically experimental stability limit for the case of the square pulse (4.14) is presented (dashed line with plus signs).*

4.4. Numerical results. We present simulation results showing PD as an upscaling of MD. In section 4.4.1, we show that the numerical dispersion appearing in MD is preserved in PD, in contrast with the CCM wave equation (4.7). In section 4.4.2, we present numerical examples demonstrating that nonlocal models are more dispersive than local models. This additional dispersion can regularize the solution, as shown in section 4.4.3.

In this section, we implement equation (A.2) for all cases (MD, PD, and CCM), taking it to be the exact MD equation of motion provided the atomistic resolution, an

appropriate quadrature for the PD equation of motion, and a suitable approximation for the CCM equation provided a high spatial resolution with a small enough horizon. This equation is evolved in time using the velocity Verlet algorithm. We will take the high resolution solutions as numerically "exact" for both PD and CCM.

4.4.1. Comparing molecular dynamics, peridynamics, and classical continuum mechanics. Following [4], we choose the domain to be $\Omega = [0, 1000]$. The initial profile is defined by $y(x, 0) = x + p(x)$ for all $x \in \Omega$, where $p(x)$ is a smooth 21st order polynomial such that $p \equiv 0$ on $[0, 490] \cup [510, 1000]$, $p(500) = 1$, and $p'(x) = p''(x) = \cdots = p^{(10)}(x) = 0$ for $x = 490, 500, 510$. We choose a specific space-time refinement path. The relation used is based on the stability condition (4.12), having the form

$$(4.13) \qquad \Delta t = \Delta t_0 \sqrt{\frac{\rho}{K(N) \sum_{i=1}^{N} \frac{1}{i}}} \Delta x,$$

with $\Delta t_0 = 0.85$ a "safety factor" chosen to ensure a stable time step.

In our numerical results, we present plots of the displacement field for specific moments in time. However, we also wish to compactly show the evolution of the system in time. To this end, we have utilized the plotting style of [4], which allows us to visualize an entire simulation, from start to finish, in a single plot. In these plots (see, for example, Figure 4.3) the x-axis represents the reference configuration (the position of each atom/particle/node in the original grid) and the y-axis represents time (from top to bottom). Each point in the plot corresponds to a given atom/particle/node at a specific time step. The color assigned to a point is a local approximation of an intensive quantity. In this case, we have used the mass density $(y')^{-1}$, computed as $(x_{j+1} - x_{j-1})/(y_{j+1} - y_{j-1})$, although any other intensive quantity could be used.

In Figure 4.3, we compare the results of (a) an MD simulation of 4,001 atoms with $N = 20$ neighbor interactions, (c) a high resolution solution of the PD model containing 100,001 particles with $N = 500$ neighbor interactions, (d) a coarse PD simulation containing 2,001 particles with $N = 10$ neighbor interactions, and (b) a CCM high resolution solution using 100,001 nodes with $N = 20$ neighbor interactions. We present in Figure 4.4 the displacement profiles of a single frame of the simulations at $t = 150.05$.

In the CCM simulation, the horizon tends to 0, producing a local model (δ-convergence [9]), in contrast to the PD simulation that keeps a constant horizon of $\delta = 5$ (m-convergence [9]), producing a nonlocal interaction. As we can see, the MD simulation produces similar dispersive effects to the "exact" PD solution, in contrast to the CCM model (4.7) in which no dispersion occurs (cf. Figures 4.3(b) and 4.4(b)). In addition, the PD approach allows us to solve our system on a coarser mesh which results in a less computationally expensive simulation. In Table 4.1, we compare the computational cost of the coarse PD simulation in relation to the MD simulation, showing that the PD simulation incurs only 1/5 the cost of the MD simulation.

4.4.2. Local vs. nonlocal models. In order to emphasize the effect of nonlocality, we run a nearest neighbor MD simulation of 1,001 atoms in comparison with an MD simulation with the same resolution, but using $N = 5$ neighbor interactions. The spring constants of the simulations are chosen so that the energy density per particle of both systems is the same; see Appendix A.1. The results are presented in Figure 4.5. Figures 4.5(a),(b) show the density evolution of the simulations, similar to Figure 4.3, whereas Figures 4.5(c),(d) present the displacement profiles of a single
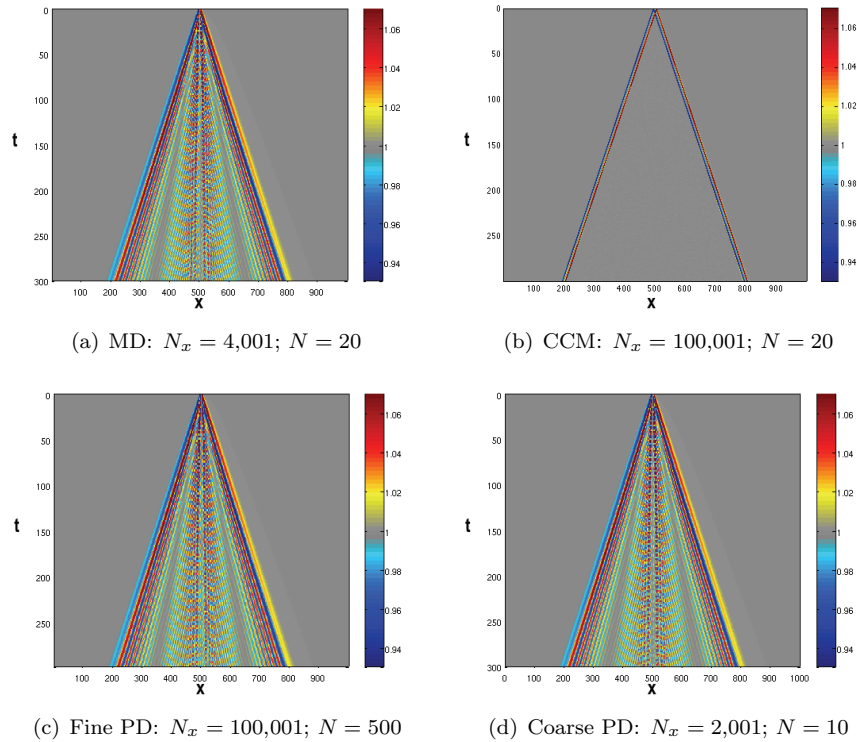
(a) MD: $N_x = 4{,}001$; $N = 20$

(b) CCM: $N_x = 100{,}001$; $N = 20$

(c) Fine PD: $N_x = 100{,}001$; $N = 500$

(d) Coarse PD: $N_x = 2{,}001$; $N = 10$

FIG. 4.3. *Density evolution for the molecular dynamics (MD), peridynamics (PD) (fine and coarse), and classical continuum mechanics (CCM) cases. Time is represented in the vertical axis (from top to bottom), and the horizontal axis represents the atom/particle/node position in the reference configuration. N_x is the number of atoms* (a), *nodes* (b), *or particles* (c), (d), *and N is the number of one-sided neighbor interactions. The simulations are evolved in time using velocity Verlet applied to* (A.2); *this equation is the exact MD equation of motion in* (a) *with ΔX the atomistic resolution, an appropriate quadrature for the PD equation of motion in* (c), (d), *and a suitable approximation for the CCM equation in* (b) *for a high spatial resolution with small enough horizon.*

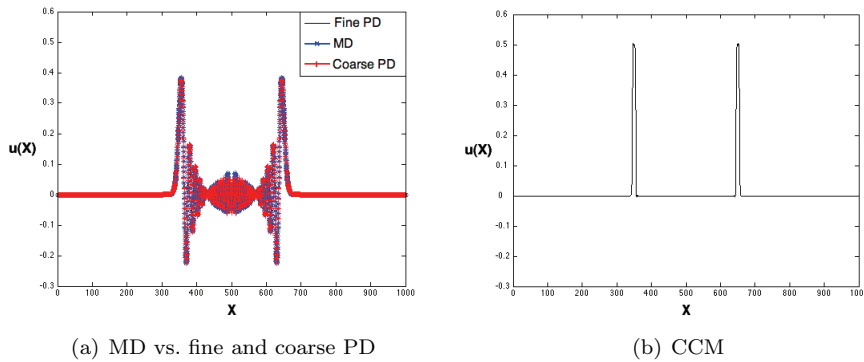(a) MD vs. fine and coarse PD

(b) CCM

FIG. 4.4. *Comparison between the displacement profiles at $t = 150.05$ for the molecular dynamics (MD), fine and coarse peridynamics (PD)* (a), *and the classical continuum mechanics (CCM)* (b) *simulations.*

TABLE 4.1

Molecular dynamics (MD) and peridynamics (PD) computational costs. N_x is the number of atoms/particles, N is the number of neighbor interactions, and N_t is the number of time steps. The cost of a simulation is estimated by the product $N_x N N_t$. The relative cost is calculated in relation to the MD simulation cost.

Model	N_x	N	N_t	Relative cost
MD	4,001	20	184	1.00
PD (coarse)	2,001	10	162	0.22

(a) MD: $N_x = 1,001$; $N = 1$

(b) MD: $N_x = 1,001$; $N = 5$

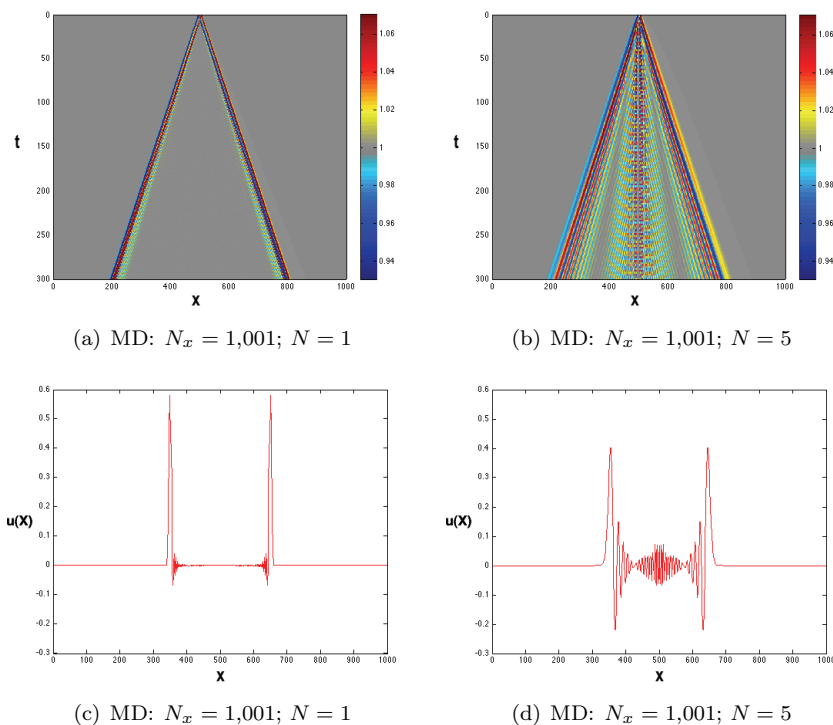(c) MD: $N_x = 1,001$; $N = 1$

(d) MD: $N_x = 1,001$; $N = 5$

FIG. 4.5. *Top: Comparison of the density evolution of molecular dynamics (MD) systems for a local interaction* (a) *and a nonlocal interaction* (b). *The axes and color interpretation are the same as in Figure* 4.3. *Bottom: Comparison of the displacement profiles of MD systems at $t = 150.45$ for a local interaction* (c) *and a nonlocal interaction* (d).

simulation frame at $t = 150.45$. We see that nonlocality (cf. Figure 4.5(b)) increases the amount of dispersion appearing in the numerical simulation, in comparison to a local interaction (cf. Figure 4.5(a)). In Figures 4.5(a),(b), dispersion is indicated by broadening. For comparison, Figures 4.3(b) and 4.4(b) display essentially no dispersion. We observe that nonlocal models are more dispersive than local models. Generally speaking, dispersion arises from both the inhomogeneities (discreteness) and the nonlocality of a system.

4.4.3. Peridynamics vs. a higher-order gradient model. In order to illustrate the advantage of PD over the HOG models, we run similar simulations as in section 4.4.1, but with a discontinuous initial condition. The initial displacement is chosen to be a square pulse defined by
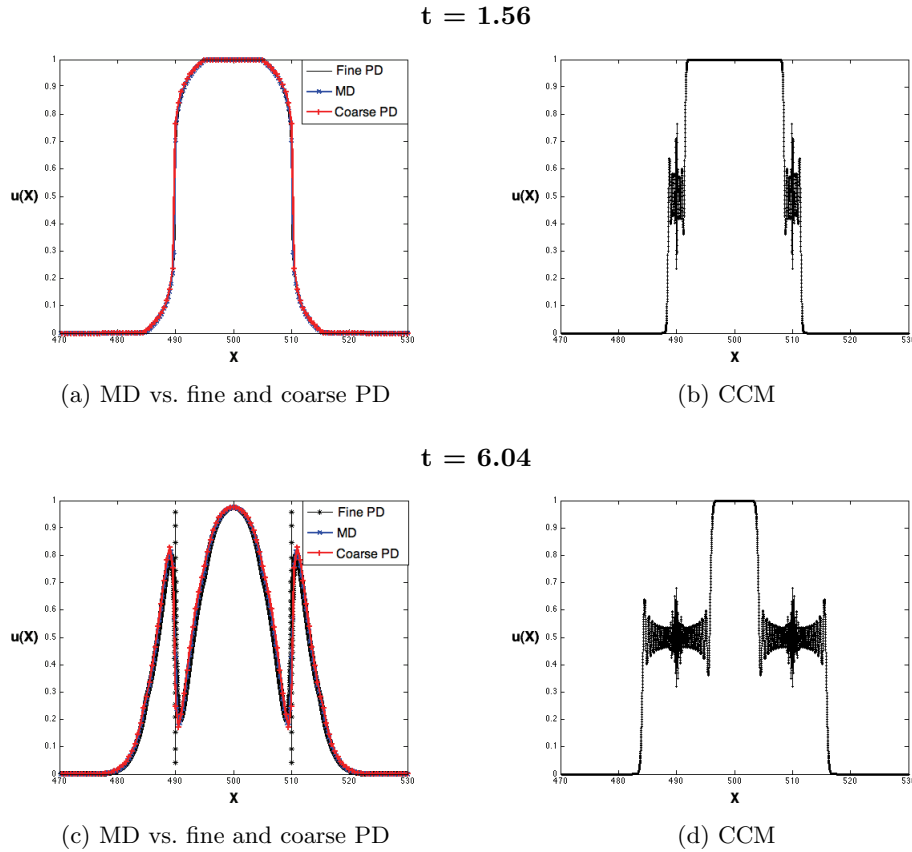
t = 1.56

(a) MD vs. fine and coarse PD

(b) CCM

t = 6.04

(c) MD vs. fine and coarse PD

(d) CCM

FIG. 4.6. *Comparison at two different times (top and bottom) of the Gibbs effect appearing in a square pulse simulation for the classical continuum mechanics (CCM) (b), (d), molecular dynamics (MD) (a), (c) (line with crosses), and fine (a), (c) (line with asterisks) and coarse (a), (c) (line with plus signs) peridynamics (PD) simulations.*

$$(4.14) \qquad u(x,0) = \left\{ \begin{array}{ll} 0, & x \in [0, 490) \cup (510, 1000], \\ 1, & x \in [490, 510]. \end{array} \right.$$

In Figure 4.6, we compare the evolution of the square pulse function for the CCM, MD, and PD models at two different times. In particular, we see agreement between the MD and PD simulations (a), (c), but a qualitatively different solution from the CCM simulation (b), (d). We notice that the CCM simulation produces large oscillations (Gibbs phenomenon) due to the jump discontinuity in the initial condition. In contrast, these oscillations are less prominent in the MD and PD simulations. For all the simulations in Figure 4.6 the same time step ($\Delta t = 0.0649$) was used, calculated using the CCM simulation parameters in (4.13).

5. Lennard-Jones model. Here we propose a PD model as an upscaling of the Lennard-Jones MD model. This PD model produces the same HOG continuum model as that obtained from the MD model, provided the same resolution is used. Because of the fast decay of the Lennard-Jones interaction, it appears that its length scale is connected to the interatomic distance, and not to the horizon, in contrast to the nonlocal linear springs MD model.

Our one-dimensional MD model consists of a linear chain of atoms interacting through a truncated Lennard-Jones potential; i.e., the number of neighbor interactions is finite. As in section 4, each atom is assumed to have mass m and is connected to N neighbors on each side, analogous to a cutoff radius used in MD simulations, although we allow N to take arbitrary values. The distance between nearest neighbors in equilibrium is assumed to be a, and the interaction is defined through the constants σ and ϵ. The equation of motion is

(5.1)

$$m\ddot{y}(x_i, t) = -\sum_{\substack{j=-N \\ j\neq 0}}^{N} 24\epsilon \left[2\frac{\sigma^{12}}{(y(x_i + ja, t) - y(x_i, t))^{13}} - \frac{\sigma^6}{(y(x_i + ja, t) - y(x_i, t))^7} \right]$$

for $i = 1, \ldots, N_x$. N_x is the number of atoms in the system, and $y(x_i, t)$ is the position at time t of an atom that was at x_i in the reference configuration.

5.1. Higher-order gradient continuum model. To develop a HOG PDE for (5.1), we first write the local potential $\Phi^{(A),\overline{x}}$ (see section 3.2) as

$$\Phi^{(A),\overline{x}} = \begin{cases} \displaystyle\sum_{j=1}^{\lfloor \frac{N}{2} \rfloor} 4\epsilon \left[\left(\frac{\sigma}{y(\overline{x} + ja, t) - y(\overline{x} - ja, t)} \right)^{12} \right. \\ \qquad\qquad \left. - \left(\frac{\sigma}{y(\overline{x} + ja, t) - y(\overline{x} - ja, t)} \right)^6 \right] \quad \text{if } \frac{\overline{x}}{a} \in \mathbb{Z} \cap \Omega, \\[20pt] \displaystyle\sum_{j=1}^{\lceil \frac{N}{2} \rceil} 4\epsilon \left[\left(\frac{\sigma}{y(\overline{x} + ja - \frac{a}{2}, t) - y(\overline{x} - ja + \frac{a}{2}, t)} \right)^{12} \right. \\ \qquad\qquad \left. - \left(\frac{\sigma}{y(\overline{x} + ja - \frac{a}{2}, t) - y(\overline{x} - ja + \frac{a}{2}, t)} \right)^6 \right] \quad \text{if } \frac{\overline{x}}{a} \in \left(\mathbb{Z} + \frac{1}{2} \right) \cap \Omega. \end{cases}$$

The inner expansion is applied as in section 4.1 to obtain the expression

$$\rho\frac{\partial^2 y}{\partial t^2} = 8\bar{\epsilon}\left[12\frac{\bar{\sigma}^{12}}{(y')^{14}} \left\{ \binom{13}{1}\left(\frac{y''}{2} + \frac{Z^N(10)}{Z^N(12)}a^2\frac{y^{(4)}}{24} + \frac{Z^N(8)}{Z^N(12)}a^4\frac{y^{(6)}}{720} \right) \right.\right.$$

$$- \frac{1}{y'}\binom{14}{2}\left(\frac{Z^N(10)}{Z^N(12)}a^2\frac{y''y'''}{6} + \frac{Z^N(8)}{Z^N(12)}a^4\left[\frac{y''y^{(5)}}{120} + \frac{y'''y^{(4)}}{72} \right] \right)$$

$$+ \frac{1}{(y')^2}\binom{15}{3}\left(\frac{Z^N(10)}{Z^N(12)}a^2\frac{(y'')^3}{8} + \frac{Z^N(8)}{Z^N(12)}a^4\left[\frac{(y'')^2y^{(4)}}{32} + \frac{y''(y''')^2}{24} \right] \right)$$

$$- \frac{1}{(y')^3}\binom{16}{4}\left(\frac{Z^N(8)}{Z^N(12)}a^4\frac{(y'')^3y'''}{12} \right) + \frac{1}{(y')^4}\binom{17}{5}\left(\frac{Z^N(8)}{Z^N(12)}a^4\frac{(y'')^5}{32} \right) \right\}$$

(5.2)

$$- 6\frac{\bar{\sigma}^6}{(y')^8}\left\{ \binom{7}{1}\left(\frac{y''}{2} + \frac{Z^N(4)}{Z^N(6)}a^2\frac{y^{(4)}}{24} + \frac{Z^N(2)}{Z^N(6)}a^4\frac{y^{(6)}}{720} \right) \right.$$

$$- \frac{1}{y'}\binom{8}{2}\left(\frac{Z^N(4)}{Z^N(6)}a^2\frac{y''y'''}{6} + \frac{Z^N(2)}{Z^N(6)}a^4\left[\frac{y''y^{(5)}}{120} + \frac{y'''y^{(4)}}{72} \right] \right)$$

$$+ \frac{1}{(y')^2}\binom{9}{3}\left(\frac{Z^N(4)}{Z^N(6)}a^2\frac{(y'')^3}{8} + \frac{Z^N(2)}{Z^N(6)}a^4\left[\frac{(y'')^2y^{(4)}}{32} + \frac{y''(y''')^2}{24} \right] \right)$$

$$\left.\left. - \frac{1}{(y')^3}\binom{10}{4}\left(\frac{Z^N(2)}{Z^N(6)}a^4\frac{(y'')^3y'''}{12} \right) + \frac{1}{(y')^4}\binom{11}{5}\left(\frac{Z^N(2)}{Z^N(6)}a^4\frac{(y'')^5}{32} \right) \right\} \right],$$

where the dependence on position and time has been omitted for simplicity; the notation $y' \equiv \partial y / \partial x$ is used as well as $y^{(n)} \equiv \frac{\partial^n y}{\partial x^n}$ for $n > 3$. Furthermore, $Z^N(n) \equiv \sum_{j=1}^{N} \frac{1}{j^n}$ is the finite analogue of the Riemann zeta function. The model parameters $\bar\sigma$ and $\bar\epsilon$ are defined as (cf. Appendix A.2)

$$\bar\sigma \equiv \left(\frac{Z^N(12)}{Z^N(6)}\right)^{1/6} \frac{\sigma}{a}, \qquad \bar\epsilon \equiv \frac{(Z^N(6))^2}{Z^N(12)} \frac{\epsilon}{a}.$$

This HOG PDE has coefficients that depend on the lattice constant a, in contrast to the nonlocal linear springs MD model where the coefficients depend on Na. In addition, because $Z^N(n)$ converges rapidly with increasing N, for $n = 6$ and $n = 12$ the dependence of the constants $\bar\sigma$ and $\bar\epsilon$ on the number of neighbor interactions N decays quickly.

5.2. Peridynamics model. A PD model corresponding to the MD model (5.1) is (cf. Appendix A.2)

(5.3)
$$\rho(x)\frac{\partial^2 y}{\partial t^2}(x,t) = -\int_{-\infty}^{\infty} 24\bar\epsilon \sum_{\substack{j=-M \\ j\neq 0}}^{M}\left[\frac{2}{j^{12}Z^M(12)}\frac{(\varepsilon\bar\sigma)^{12}}{(y(x+\varepsilon,t)-y(x,t))^{13}}\right.$$
$$\left. -\frac{1}{j^6 Z^M(6)}\frac{(\varepsilon\bar\sigma)^6}{(y(x+\varepsilon,t)-y(x,t))^7}\right]\Delta(\varepsilon - j\Delta x)d\varepsilon,$$
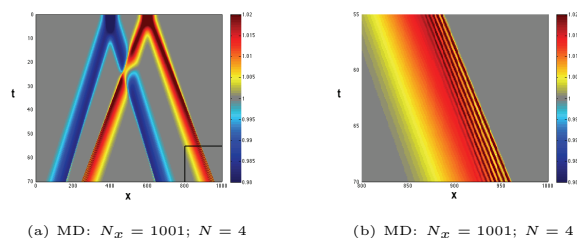
with $\Delta(x)$ the Dirac delta function,[3] M the chosen number of neighbor interactions, and Δx the chosen spatial resolution for the model.

The HOG continuum model derived from (5.3) is identical to (5.2) if $M = N$ and $\Delta x = a$, and has the form

$$\rho\frac{\partial^2 y}{\partial t^2} = 8\bar\epsilon\left[12\frac{\bar\sigma^{12}}{(y')^{14}}\left\{\binom{13}{1}\left(\frac{y''}{2} + \frac{Z^M(10)}{Z^M(12)}(\Delta x)^2\frac{y^{(4)}}{24} + \frac{Z^M(8)}{Z^M(12)}(\Delta x)^4\frac{y^{(6)}}{720}\right)\right.\right.$$

$$-\frac{1}{y'}\binom{14}{2}\left(\frac{Z^M(10)}{Z^M(12)}(\Delta x)^2\frac{y''y'''}{6} + \frac{Z^M(8)}{Z^M(12)}(\Delta x)^4\left[\frac{y''y^{(5)}}{120} + \frac{y'''y^{(4)}}{72}\right]\right)$$

$$+\frac{1}{(y')^2}\binom{15}{3}\left(\frac{Z^M(10)}{Z^M(12)}(\Delta x)^2\frac{(y'')^3}{8} + \frac{Z^M(8)}{Z^M(12)}(\Delta x)^4\left[\frac{(y'')^2 y^{(4)}}{32} + \frac{y''(y''')^2}{24}\right]\right)$$

$$\left.-\frac{1}{(y')^3}\binom{16}{4}\left(\frac{Z^M(8)}{Z^M(12)}(\Delta x)^4\frac{(y'')^3 y'''}{12}\right) + \frac{1}{(y')^4}\binom{17}{5}\left(\frac{Z^M(8)}{Z^M(12)}(\Delta x)^4\frac{(y'')^5}{32}\right)\right\}$$

$$-6\frac{\bar\sigma^6}{(y')^8}\left\{\binom{7}{1}\left(\frac{y''}{2} + \frac{Z^M(4)}{Z^M(6)}(\Delta x)^2\frac{y^{(4)}}{24} + \frac{Z^M(2)}{Z^M(6)}(\Delta x)^4\frac{y^{(6)}}{720}\right)\right.$$

(5.4)
$$-\frac{1}{y'}\binom{8}{2}\left(\frac{Z^M(4)}{Z^M(6)}(\Delta x)^2\frac{y''y'''}{6} + \frac{Z^M(2)}{Z^M(6)}(\Delta x)^4\left[\frac{y''y^{(5)}}{120} + \frac{y'''y^{(4)}}{72}\right]\right)$$

$$+\frac{1}{(y')^2}\binom{9}{3}\left(\frac{Z^M(4)}{Z^M(6)}(\Delta x)^2\frac{(y'')^3}{8} + \frac{Z^M(2)}{Z^M(6)}(\Delta x)^4\left[\frac{(y'')^2 y^{(4)}}{32} + \frac{y''(y''')^2}{24}\right]\right)$$

$$\left.\left.-\frac{1}{(y')^3}\binom{10}{4}\left(\frac{Z^M(2)}{Z^M(6)}(\Delta x)^4\frac{(y'')^3 y'''}{12}\right) + \frac{1}{(y')^4}\binom{11}{5}\left(\frac{Z^M(2)}{Z^M(6)}(\Delta x)^4\frac{(y'')^5}{32}\right)\right\}\right].$$

---

[3]We have reserved the symbol δ for the PD horizon (cf. section 2).

Molecular Dynamics

(a) MD: $N_x = 1001$; $N = 4$ (b) MD: $N_x = 1001$; $N = 4$

Peridynamics

(c) PD: $N_x = 1001$; $N = 4$ (d) Coarse PD: $N_x = 501$; $N = 2$ (e) Coarse PD: $N_x = 251$; $N = 1$
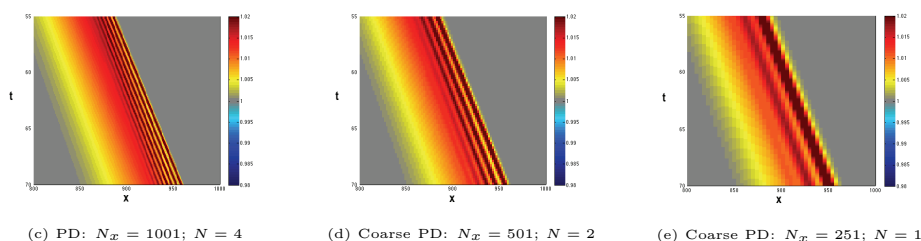
FIG. 5.1. *Density evolution for the molecular dynamics (MD)* (a), (b) *and peridynamics (PD)* (c), (d), (e) *simulations. The axes and color interpretation are the same as in Figure* 4.3 *(see section* 4.4.1*).* (b) *and* (c), (d), (e) *are a zoom-in of the bottom-right corner of* (a), *and show the dispersion patterns produced by the shock.*

5.3. Numerical experiments. For our simulations, we utilize the same plot style and same computational domain as in section 4.4. Even for a smooth initial condition, the Lennard-Jones model will typically exhibit shocks after some time due to the nonlinearity of the model. To emphasize the shock evolution, we choose an initial profile similar to that in section 4.4 but with twice the amplitude. For the PD simulations, we choose a particular refinement/coarsening path such that $\Delta x = na$ and $M = N/n$, where n is an integer.[4] Note that for $n = 1$, we recover (5.1). A comparison between the MD and PD models is presented in Figure 5.1, where we show (a), (b) an MD simulation for 1,001 atoms with $N = 4$ neighbor interactions, (c) a PD simulation with the same resolution and number of neighbor interactions, (d) a coarse PD simulation with 501 particles and $N = 2$ neighbor interactions, and (e) a coarse PD simulation with 251 particles with only a nearest neighbor interaction. Figure 5.1(a) shows the MD simulation on the complete space-time domain. The remaining plots show a zoom-in of the bottom-right corner of Figure 5.1(a) to better illustrate the solution near the shock front. We omit the entire space-time domain PD plots since they are qualitatively similar to the MD plot. Figure 5.1(b) shows the MD simulation results. The PD simulations are shown in Figures 5.1(c), (d), (e). In this case, we choose a uniform stable time step of $\Delta t = 0.1$ for all simulations. The PD model reproduces the dispersion and shock effects appearing in the MD simulation,

---

[4]In this paper, the discretization of [28] is used. If the PD horizon is held constant, the interparticle distance cannot exceed the horizon, otherwise the particles would be disconnected from each other. This is a limitation of the specific discretization used, and not of the PD model itself. Many other discretizations can be used; see [13]. This issue is of particular interest for the short-range interactions considered in this paper. A discretization that is coarse with respect to the PD horizon is effectively local. This is to be expected, as small-scale spatial inhomogeneities become negligible at large scales.
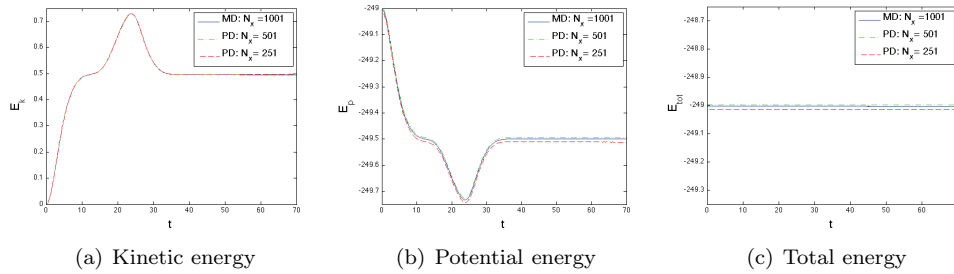
(a) Kinetic energy   (b) Potential energy   (c) Total energy

FIG. 5.2. *Comparison of the kinetic* (a), *potential* (b), *and total energy* (c) *between the molecular dynamics (MD) and coarse peridynamics (PD) simulations.*

given the same resolution. The PD solution at the shock front changes with the discretization.

In Figure 5.2, we show energy conservation for the PD (fine and coarse) models. As the PD model was derived under the constraint that energy is preserved (see Appendix A.2), these numerical results are consistent with the theory.

6. Concluding remarks. We have introduced peridynamics (PD) as an upscaling of molecular dynamics (MD). PD models have been presented for both nonlocal linear springs and Lennard-Jones MD models, and the correspondence between the MD and PD models was established through the comparison of corresponding higher-order gradient (HOG) models.

For the nonlocal linear springs model, we have shown that the dispersion relations and HOG PDE obtained from MD and PD are consistent to arbitrary order if the horizon is held constant. In particular, we have presented numerical experiments showing that the dispersion present in MD models is preserved in PD models, but lost in classical continuum mechanics models. We have shown that nonlocal models are more dispersive than local models. Furthermore, nonlocality was shown to produce a smoothing effect in simulations with discontinuous initial conditions.

We have also presented a PD model that is an upscaling of the Lennard-Jones MD model. We have shown that the proposed PD model can recover the same dynamics as the MD model by choosing the appropriate length scale. In contrast to the nonlocal linear springs model, where the length scale is determined by the horizon of the interaction (i.e., the maximum interaction distance), in the Lennard-Jones models, the interatomic spacing sets the length scale. As the PD model recovers the MD results for an atomistic resolution, this work provides a natural framework for mesh-refinement applications.

Appendix A. Derivation of peridynamics models. We seek PD models with dynamics similar to that of MD models. This process implies the derivation of a continuum model composed of a kernel function $\boldsymbol{\kappa}$ under an integral. The problem of deriving a continuous PD model from a discrete MD model involves first finding a generalized discrete model consistent with the specific MD model, and then producing a continuum formulation from that generalized discrete model. In this section, we present the derivation of the PD models for nonlocal linear springs and Lennard-Jones MD models.

A.1. Nonlocal linear springs model. The nonlocal linear springs MD model was presented in (4.1). The potential energy density of a particle in a chain with

resolution Δx having M neighbor interactions is

$$\varphi(x,t) = \sum_{\substack{j=-M \\ j\neq 0}}^{M} \frac{1}{\Delta x}\frac{1}{2}\frac{K(M)}{|j\Delta x|}\left(y(x+j\Delta x,t) - y(x,t) - j\Delta x\right)^2.$$

Assuming an isotropic deformation such that $y(x,t) - x = \alpha x$,

$$(A.1) \qquad \varphi(x,t) = \alpha^2 K(M)\frac{M(M+1)}{2}.$$

The general approach is to match the energy density per particle between systems containing different numbers of particles and neighbor interactions. To achieve that, we find the relation between the constant $K(M)$ for M neighbor interactions with the constant $K(1)$ for a nearest neighbor interaction under the same deformation by using (A.1). Then, systems with different numbers of neighbor interactions can be related through a "reference" nearest neighbor system. We denote $K_1 \equiv K(1)$ and obtain the following relation:

$$K(M) = \frac{2}{M(M+1)}K_1.$$

This allows us to write a generalized equation of motion as

(A.2)

$$\rho(x)\frac{\partial^2 y}{\partial t^2}(x,t) = \sum_{\substack{j=-M \\ j\neq 0}}^{M} \frac{2K_1}{|j\Delta x|M(M+1)(\Delta x)^2}\left(y(x+j\Delta x,t) - y(x,t) - j\Delta x\right)\Delta x.$$

Taking the above expression as a quadrature of an integral, we obtain (in the limit $M \gg 1$ and $\Delta x \ll 1$ such that $M\Delta x = \delta$) the expression

$$(A.3) \qquad \rho(x)\frac{\partial^2 y}{\partial t^2}(x,t) = \int_{-\delta}^{\delta}\frac{c}{|\varepsilon|}\left(y(x+\varepsilon,t) - y(x,t) - \varepsilon\right)\mathrm{d}\varepsilon,$$

where $c = 2K_1/\delta^2$, and we have used the following substitutions: $\Delta x \to \mathrm{d}\varepsilon$, $j\Delta x \to \varepsilon$. This gives us a PD model that upscales the nonlocal linear springs MD model.

A.2. Lennard-Jones model. The Lennard-Jones MD model was presented in (5.1). The potential energy density of a particle in a chain with resolution Δx having M neighbor interactions is

$$\varphi(x,t) = \sum_{\substack{j=-M \\ j\neq 0}}^{M} \frac{1}{\Delta x}4\epsilon(M)\left[\left(\frac{\sigma(M)}{y(x+j\Delta x,t) - y(x,t)}\right)^{12} - \left(\frac{\sigma(M)}{y(x+j\Delta x,t) - y(x,t)}\right)^{6}\right],$$

where for convenience we write the dependence of the interaction constants ϵ and σ on the number of neighbor interactions. Assuming the system is in equilibrium in the reference configuration, we can write

$$(A.4) \qquad \varphi(x,0) = \sum_{\substack{j=-M \\ j\neq 0}}^{M} \frac{1}{\Delta x}4\epsilon(M)\left[\left(\frac{\sigma(M)}{j\Delta x}\right)^{12} - \left(\frac{\sigma(M)}{j\Delta x}\right)^{6}\right].$$

We realize that $\sigma(M)$ determines a length scale. Thus, we would like to know the relation between $\sigma(M)$ and the nearest neighbor distance, in the equilibrium configuration, Δx. Assuming the system is in equilibrium, we minimize the potential energy density with respect to the length scale constant such that $\frac{\partial \varphi}{\partial \sigma(M)} = 0$ to get

$$(A.5) \qquad \sigma(M) = \left(\frac{Z^M(6)}{Z^M(12)} \right)^{1/6} \frac{1}{2^{1/6}} \Delta x.$$

To find the relation between the length scale constant of nearest neighbor interaction $\sigma(1)$ and that of the M neighbor interaction $\sigma(M)$, we use (A.5) and assume $\Delta x = C r_1$, with r_1 the nearest neighbor equilibrium distance for a nearest neighbor interaction, and C a refinement factor. We get

$$(A.6) \qquad \sigma(M) = \Delta x \left(\frac{Z^M(6)}{Z^M(12)} \right)^{1/6} \overline{\sigma},$$

where $\overline{\sigma} = \sigma(1)/r_1$ is a constant.

So far we have found a relation between the length scale constants so that we obtain consistency with the refinement process. We now find the relation between the energy constants in order to match the energy densities. We substitute the relation (A.6) in (A.4) to get

$$\varphi(x,0) = 8 \frac{\epsilon(M)}{\Delta x} \frac{\left(Z^M(6)\right)^2}{Z^M(12)} \left[\overline{\sigma}^{12} - \overline{\sigma}^6 \right].$$

Comparing with a nearest neighbor interaction, we obtain

$$\epsilon(M) = \Delta x \frac{Z^M(12)}{\left(Z^M(6)\right)^2} \overline{\epsilon},$$

with $\overline{\epsilon} = \epsilon(1)/r_1$. The general expression for the equation of motion is

$$\rho(x) \frac{\partial^2 y}{\partial t^2}(x,t) = - \sum_{\substack{j=-M \\ j \neq 0}}^{M} 24 \overline{\epsilon} \left[\frac{2}{Z^M(12)} \frac{(\Delta x \overline{\sigma})^{12}}{(y(x+j\Delta x,t) - y(x,t))^{13}} \right. $$
$$\left. - \frac{1}{Z^M(6)} \frac{(\Delta x \overline{\sigma})^6}{(y(x+j\Delta x,t) - y(x,t))^7} \right].$$

We can write the above equation as the continuum expression

$$\rho(x) \frac{\partial^2 y}{\partial t^2}(x,t) = - \int_{-\infty}^{\infty} 24 \overline{\epsilon} \sum_{\substack{j=-M \\ j \neq 0}}^{M} \left[\frac{2}{j^{12} Z^M(12)} \frac{(\varepsilon \overline{\sigma})^{12}}{(y(x+\varepsilon,t) - y(x,t))^{13}} \right. $$
$$\left. - \frac{1}{j^6 Z^M(6)} \frac{(\varepsilon \overline{\sigma})^6}{(y(x+\varepsilon,t) - y(x,t))^7} \right] \Delta(\varepsilon - j\Delta x) d\varepsilon,$$

with the Dirac delta function $\Delta(x)$.[5] This gives us a PD model that upscales the Lennard-Jones MD model.

---

[5] The idea of using Dirac delta functions for the continualization process was inspired by [19].

REFERENCES

[1] E. C. Aifantis, *Gradient deformation models at nano, micro, and macro scales*, J. Eng. Mater. Technol., 121 (1999), pp. 189–202.

[2] I. V. Andrianov and J. Awrejcewicz, *Continuous models for 1D discrete media valid for higher-frequency domain*, Phys. Lett. A, 345 (2005), pp. 55–62.

[3] M. Arndt, *Upscaling from Atomistic Models to Higher Order Gradient Continuum Models for Crystalline Solids*, Ph.D. thesis, Institute for Numerical Simulation, University of Bonn, Bonn, Germany, 2004.

[4] M. Arndt and M. Griebel, *Derivation of higher order gradient continuum models from atomistic models for crystalline solids*, Multiscale Model. Simul., 4 (2005), pp. 531–562.

[5] E. Askari, F. Bobaru, R. B. Lehoucq, M. L. Parks, S. A. Silling, and O. Weckner, *Peridynamics for multiscale materials modeling*, J. Phys. Conf. Ser., 125 (2008), article 012078.

[6] H. Askes and A. V. Metrikine, *Higher-order continua derived from discrete media: Continualisation aspects and boundary conditions*, Internat. J. Solids Structures, 42 (2005), pp. 187–202.

[7] S. Bardenhagen and N. Triantafyllidis, *Derivation of higher order gradient continuum theories in 2,3-d nonlinear elasticity from periodic lattice models*, J. Mech. Phys. Solids, 42 (1994), pp. 111–139.

[8] G. I. Barenblatt, *Scaling, Self-Similarity, and Intermediate Asymptotics*, Cambridge Texts Appl. Math. 14, Cambridge University Press, Cambridge, UK, 1996.

[9] F. Bobaru, M. Yang, L. F. Alves, S. A. Silling, E. Askari, and J. Xu, *Convergence, adaptive refinement, and scaling in 1D peridynamics*, Internat. J. Numer. Methods Engrg., 77 (2009), pp. 852–877.

[10] C. S. Chang, H. Askes, and L. J. Sluys, *Higher-order strain/higher-order stress gradient models derived from a discrete microstructure, with application to fracture*, Eng. Fract. Mech., 69 (2002), pp. 1907–1924.

[11] W. Chen and J. Fish, *A dispersive model for wave propagation in periodic heterogeneous media based on homogenization with multiple spatial and temporal scales*, J. Appl. Mech., 68 (2001), pp. 153–161.

[12] E. Emmrich and O. Weckner, *On the well-posedness of the linear peridynamic model and its convergence towards the Navier equation of linear elasticity*, Commun. Math. Sci., 5 (2007), pp. 851–864.

[13] E. Emmrich and O. Weckner, *The peridynamic equation and its spatial discretisation*, Math. Model. Anal., 12 (2007), pp. 17–27.

[14] E. Hairer, C. Lubich, and G. Wanner, *Geometric numerical integration illustrated by the Störmer/Verlet method*, Acta Numer., 12 (2003), pp. 1–51.

[15] E. Kröner, *Elasticity theory of materials with long range cohesive forces*, Internat. J. Solids Structures, 3 (1967), pp. 731–742.

[16] M. D. Kruskal and N. J. Zabusky, *Stroboscopic-perturbation procedure for treating a class of nonlinear wave equations*, J. Math. Phys., 5 (1964), pp. 231–244.

[17] I. A. Kunin, *Elastic Media with Microstructure* I: *One-Dimensional Models*, Springer Ser. Solid-State Sci. 26, Springer-Verlag, Berlin, 1982.

[18] I. A. Kunin, *Elastic Media with Microstructure* II: *Three-Dimensional Models*, Springer Ser. Solid-State Sci. 44, Springer-Verlag, Berlin, 1983.

[19] R. B. Lehoucq and S. A. Silling, *Statistical Coarse-Graining of Molecular Dynamics into Peridynamics*, Technical report SAND2007-6410, Sandia National Laboratories, Albuquerque, 2007.

[20] A. V. Metrikine and H. Askes, *An isotropic dynamically consistent gradient elasticity model derived from a 2D lattice*, Phil. Mag., 86 (2006), pp. 3259–3286.

[21] H.-B. Mühlhaus and F. Oka, *Dispersion and wave propagation in discrete and continuous models for granular materials*, Internat. J. Solids Structures, 33 (1996), pp. 2841–2858.

[22] M. L. Parks, R. B. Lehoucq, S. J. Plimpton, and S. A. Silling, *Implementing peridynamics within a molecular dynamics code*, Comput. Phys. Comm., 179 (2008), pp. 777–783.

[23] D. Rogula, *Introduction to nonlocal theory of material media*, in Nonlocal Theory of Material Media, D. Rogula, ed., Springer-Verlag, Berlin, 1982, pp. 125–222.

[24] P. ROSENAU, *Dynamics of nonlinear mass-spring chains near the continuum limit*, Phys. Lett. A, 118 (1986), pp. 222–227.

[25] P. ROSENAU, *Hamiltonian dynamics of dense chains and lattices: Or how to correct the continuum*, Phys. Lett. A, 311 (2003), pp. 39–52.

[26] M. B. RUBIN, P. ROSENAU, AND O. GOTTLIEB, *Continuum model of dispersion caused by an inherent material characteristic length*, J. Appl. Phys., 77 (1995), pp. 4054–4063.

[27] S. A. SILLING, *Reformulation of elasticity theory for discontinuities and long-range forces*, J. Mech. Phys. Solids, 48 (2000), pp. 175–209.

[28] S. A. SILLING AND E. ASKARI, *A meshfree method based on the peridynamic model of solid mechanics*, Comput. & Structures, 83 (2005), pp. 1526–1535.

[29] S. A. SILLING, M. EPTON, O. WECKNER, J. XU, AND E. ASKARI, *Peridynamic states and constitutive modeling*, J. Elasticity, 88 (2007), pp. 151–184.

[30] S. A. SILLING AND R. B. LEHOUCQ, *Convergence of peridynamics to classical elasticity theory*, J. Elasticity, 93 (2008), pp. 13–37.

[31] A. S. J. SUIKER, R. DE BORST, AND C. S. CHANG, *Micro-mechanical modelling of granular material. Part 1: Derivation of a second-gradient micro-polar constitutive theory*, Acta Mech., 149 (2001), pp. 161–180.

[32] A. S. J. SUIKER, R. DE BORST, AND C. S. CHANG, *Micro-mechanical modelling of granular material. Part 2: Plane wave propagation in infinite media*, Acta Mech., 149 (2001), pp. 181–200.

[33] N. TRIANTAFYLLIDIS AND S. BARDENHAGEN, *On higher order gradient continuum theories in 1-D nonlinear elasticity. Derivation from and comparison to the corresponding discrete models*, J. Elasticity, 33 (1993), pp. 259–293.

[34] N. TRIANTAFYLLIDIS AND S. BARDENHAGEN, *The influence of scale size on the stability of periodic solids and the role of associated higher order gradient continuum models*, J. Mech. Phys. Solids, 44 (1996), pp. 1891–1928.

[35] O. WECKNER AND R. ABEYARATNE, *The effect of long-range forces on the dynamics of a bar*, J. Mech. Phys. Solids, 53 (2005), pp. 705–728.

[36] N. J. ZABUSKY AND M. D. KRUSKAL, *Interaction of "solitons" in a collisionless plasma and the recurrence of initial states*, Phys. Rev. Lett., 15 (1965), pp. 240–243.